

Broadband and wide-angle plane focal surface Luneburg lens

Jue Li(李珏), Yangyang Zhou(周杨阳), and Huanyang Chen(陈焕阳)
Citation: Chin. Phys. B, 2023, 32 (**6**): 064210. DOI: 10.1088/1674-1056/ac8e9e
Journal homepage: http://cpb.iphy.ac.cn; http://iopscience.iop.org/cpb

What follows is a list of articles you may be interested in

Nonreciprocal wide-angle bidirectional absorber based on one-dimensional magnetized gyromagnetic photonic crystals

You-Ming Liu(刘又铭), Yuan-Kun Shi(史源坤), Ban-Fei Wan(万宝飞), Dan Zhang(张丹), and Hai-Feng Zhang(章海锋)
Chin. Phys. B, 2023, 32 (**4**): 044203. DOI: 10.1088/1674-1056/ac921d

Large aperture phase-coded diffractive lens for achromatic and 16° field-of-view imaging with high efficiency

Gu Ma(马顾), Peng-Lei Zheng(郑鹏磊), Zheng-Wen Hu(胡正文), Suo-Dong Ma(马锁冬), Feng Xu(许峰), Dong-Lin Pu(浦东林), and Qin-Hua Wang(王钦华)
Chin. Phys. B, 2022, 31 (**7**): 074210. DOI: 10.1088/1674-1056/ac560c

Temperature-responded tunable metalenses based on phase transition materials

Jing-Jun Wu(伍景军), Feng Tang(唐烽), Jun Ma(马骏), Bing Han(韩冰), Cong Wei(魏聪), Qing-Zhi Li(李青芝), Jun Chen(陈骏), Ning Zhang(张宁), Xin Ye(叶鑫), Wan-Guo Zheng(郑万国)‡, and Ri-Hong Zhu(朱日宏)
Chin. Phys. B, 2022, 31 (**5**): 054216. DOI: 10.1088/1674-1056/ac3cad

Simple and universal method in designs of high-efficiency diffractive optical elements for spectrum separation and beam concentration

Wen-Qi Xu(徐文琪), Dong-Feng Lin(林冬风), Xin Xu(许信), Jia-Sheng Ye(叶佳声), Xin-Ke Wang(王新柯), Sheng-Fei Feng(冯胜飞), Wen-Feng Sun(孙文峰), Peng Han(韩鹏), Yan Zhang(张岩), Qing-Bo Meng(孟庆波), Guo-Zhen Yang(杨国桢)
Chin. Phys. B, 2017, 26 (**7**): 074202. DOI: 10.1088/1674-1056/26/7/074202

A single diffractive optical element implementing spectrum-splitting and beam-concentration functions simultaneously with high diffraction efficiency

Ye Jia-Sheng (叶佳声), Wang Jin-Ze (王进泽), Huang Qing-Li (黄庆礼), Dong Bi-Zhen (董碧珍), Zhang Yan (张岩), Yang Guo-Zhen (杨国桢)
Chin. Phys. B, 2013, 22 (**3**): 034201. DOI: 10.1088/1674-1056/22/3/034201

SPECIAL TOPIC — Celebrating the 100th Anniversary of Physics Discipline of Xiamen University

Broadband and wide-angle plane focal surface Luneburg lens

Jue Li(李珏)[1,2], Yangyang Zhou(周杨阳)[1,2,†], and Huanyang Chen(陈焕阳)[1,2,‡]

[1] *Institute of Electromagnetics and Acoustics and Department of Physics, College of Physical Science and Technology, Xiamen University, Xiamen* 361005, *China*

[2] *Fujian Engineering Research Center for EDA, Fujian Provincial Key Laboratory of Electromagnetic Wave Science and Detection Technology, Xiamen Key Laboratory of Multiphysics Electronic Information, Xiamen University, Xiamen* 361005, *China*

(Received 24 April 2022; revised manuscript received 4 August 2022; accepted manuscript online 2 September 2022)

The energy crisis has aroused widespread concern, and the reform of energy structure is imminent. In the future, the energy structure will be dominated by the solar energy and other renewable energy sources. The solar concentrating technology as a promising method has been widely studied for collecting solar energy. However, the previous solar concentrating technologies suffer from some drawbacks, such as low focusing efficiency and large concentrating size. The Luneburg lens with highly efficient aberration-free focusing provides a new route for solar/energy concentrator. In this work, we designed a plane focal surface Luneburg lens (PFSLL) by transformation optics (TO). The PFSLL provides a relatively high focusing efficiency and concentration ratio of collection of energy. At the same time, it circumvents the disadvantage of curve surface of the classical Luneburg lens in device integration. Based on the reciprocity of electromagnetic waves, the PFSLL can also be applied to the antenna field to achieve broadband wide-angle scanning and highly directional radiation.

Keywords: plane focal surface Luneburg lens (PFSLL), focusing efficiency, concentration ratio of collection of energy

PACS: 42.25.–p **DOI:** 10.1088/1674-1056/ac8e9e

1. Introduction

With the reality of dwindling non-renewable resource reserves, the world continues to focus on renewable energy technology development in hopes of filling the huge energy gap. Between them, solar energy as a clean, inexhaustible and reliable energy has aroused much attention in the development of renewable energy field. Solar energy technology has been developing currently involving photovoltaic (PV)[1,2] and concentrating solar power (CSP).[3–6] PV utilizes large optical elements to collect solar energy directly and then transfers it to small PV cells. This commercial technology has been developing swiftly and gaining worldwide recognition.[7–9] Nevertheless, PV systems have cost and connectivity issues.[10] CSP technology is also cost-reducing method and now there are mainly linear Fresnel reflectors (LFR),[11–13] parabolic trough collectors (PTC),[14–16] *etc.* However, CSP technology exists disadvantages of low focusing efficiency and large concentrator size.

On the one hand, metalens with light weight and photonic crystal plat lenses with scatter-size gradient has attracted much attention.[17–21] They have provided unprecedented approach to planar focusing, leading to intriguing applications such as light collector. However, their high focusing efficiency and broadband are relative, and there are still certain limitations. The Luneburg lens (LL)[22] is an ultra-broadband wide-angle aberration-free focusing lens,[23] which may provide an alternative way for the solar collector. With superior beam focusing and beam coherence, the LL can be widely used in directional radar,[24,25] optical imaging,[26] and antenna.[27,28] As a solar collector, the classical LL is disadvantaged to be realized highly efficient energy collecting and integration system on account of the curve focusing surface and low concentration ratio. To solve these problems, an LL with plane focal surface is an applicable alternative.

In this work, we designed a plane focal surface Luneburg lens (PFSLL) by the Schwarz–Christoffel (SC) method.[29–31] Through simulation, we find that the PFSLL has a relatively high focusing efficiency and concentration ratio of collection of solar energy. According the reciprocity of electromagnetic wave, the PFSLL as an antenna field can achieve broadband wide-angle scanning and highly directional far-field radiation. The PFSLL may provide a way to highly efficient solar collector and wide-angle multi-beam antenna.

2. Result

LL with gradient refractive index distribution can convert a point source into plane wave, as shown in Fig. 1(a).[23,32] The refractive index profile of classical LL located at the physical space $z = x + \mathrm{i}y$ is governed by the formula

$$n_z = \sqrt{2 - \left(\frac{r}{R}\right)^2}, \tag{1}$$

†Corresponding author. E-mail: zhouyangyang@stu.xmu.edu.cn

‡Corresponding author. E-mail: kenyon@xmu.edu.cn

© 2023 Chinese Physical Society and IOP Publishing Ltd

where $r=\sqrt{x^2+y^2}$ represents the distance from a fixed point to the center of LL, R is the radius of the lens. The LL has excellent ability of beam focusing or collimation. However, the curve surface of the classical LL is unsuitable for energy collector miniaturization and integration system. To facilitate the integration and achieve excellent concentrating performance, we redesigned a PFSLL based on the SC conformal mapping.[29] In the design, two spaces are involved: the physical space (Fig. 1(b)) and the virtual space (Figs. 1(d)–1(f)) based on conformal TO (CTO).[33] A classical LL with gradient refractive index profile and radius $R=1$ (Figs. 1(a) and 1(b)) is located at the physical space $z=x+\mathrm{i}y$. According to the SC approach, the LL could be mapped into a PFSLL in virtual space $w=u+\mathrm{i}v$, and the structure after transformation is shown in Fig. 1(c). In the figure, the flat plate width of the PFSLL is d, and the semicircle has a radius 1. Its center is at $(0,0)$. This transformation is achieved by directly compressing the semicircle of the classical LL into plane AB that make up the focal plane of lens, and the mapping function is numerically calculated by the SC program.[34] It is worth noting that the orthogonal grid in the direction in Fig. 1(b) is conformally transformed to obtain the orthogonal network shown in Figs. 1(d)–1(f) respectively, thus obtaining PFSLL with different plates of width d. The approximate refractive index of PFSLL can be given by

$$n_w = n_z / \left|f'\right|^2, \tag{2}$$

where n_z is the refractive index of the classical LL as shown in Eq. (1), and f' represents the derivative of the analytic function.[35] The refractive index distributions of PFSLL with d of 0.5, 0.4, and 0.3 respectively are corresponding to Figs. 1(d)–1(f). It shows that as the PFSLL's plate width decreases, the refractive index increases. Thus, it means that the impedance mismatch between the lens and air interface increases. At the same time, the spatial range of refractive index less than 1 becomes larger, which will also cause more scattering during the focusing process.

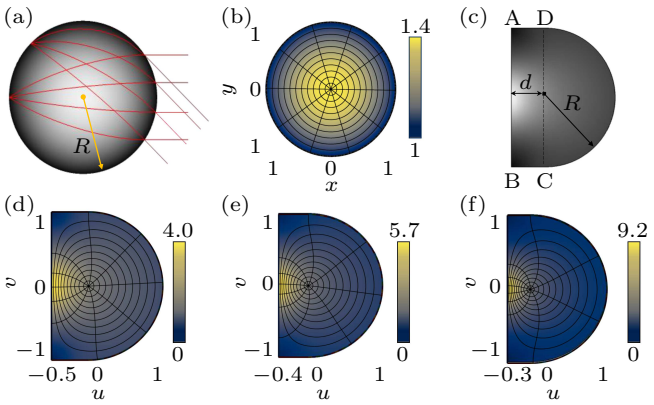


Fig. 1. (a) Geometrical optical properties of Luneburg lens (LL). (b) Refractive index distribution and orthogonal grid of LL in physical space. (c) The structure of plane focal surface Luneburg lens (PFSLL) with a plate width d in the virtual space. (d)–(f) The refractive index distribution and transformed orthogonal grid of PFSLL with plate width d of 0.5, 0.4, and 0.3 (in arbitrary units) in the virtual space respectively.

To explore the change of focusing region with respect to the plate width d of PFSLL, full wave numerical simulations are performed by commercial software COMSOL Multiphysics. It is well known that the optical path is reversible. Thus, here we only discuss the case of point source incidence. Figure 2 shows the z component of the electric fields in PFSLL with different plate widths d at the frequencies of 150 GHz, respectively. Figures 2(a) and 2(d) show the z component of the electric fields in PFSLL with flat plate width of 0.5 cm when the point source is located at (−0.5 cm, 0 cm) and (−0.5 cm, 0.1 cm), respectively. It is found that the angle of beam scanning on the other side changes with the distance from the point source to the central axis (u axis). When the point source is placed on the focal surface AB at different distances of 0 cm and 0.1 cm from the u axis, figures 2(b) and 2(e) and figures 2(c) and 2(f) show the z component of the electric fields in PFSLL with flat plate width d of 0.4 cm and 0.3 cm, respectively. From Figs. 2(d)–2(f), it reveals that the beam scanning angle of PFSLL increases with the plate width d decreases from 0.5 cm to 0.3 cm. That is, a compact focusing region of PFSLL can be achieved by shrinking the plate width d. However, it should also be noted that there is more scattering when the beam is generated on the other side of lens, with the plate width decreasing. The degree of impedance mismatch between the lens and air interface and the scattering loss both increases. Therefore, it is essential to choose an appropriate width d of PFSLL to avoid excessive energy loss in solar concentrator or antenna systems.

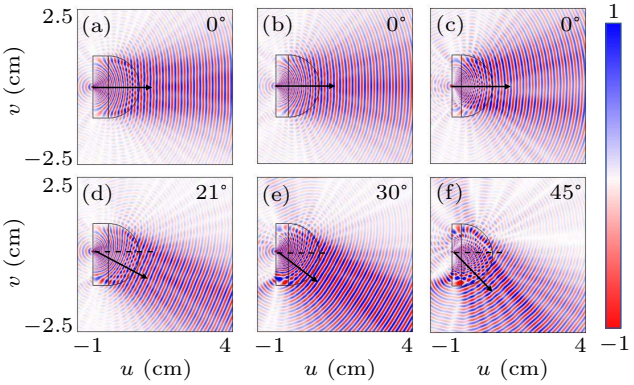


Fig. 2. The z component of the electric field of PFSLL with different plate width d at the frequencies of 150 GHz. (a) and (d) The PFSLL with a plate width d of 0.5 cm when the point source is located at (−0.5 cm, 0 cm) and (−0.5 cm, 0.1 cm). (b) and (e) The PFSLL with a plate width d of 0.4 cm when the point source is located at (−0.4 cm, 0 cm) and (−0.4 cm, 0.1 cm). (c) and (f) The PFSLL with a plate width d of 0.3 cm when the point source is located at (−0.3 cm, 0 cm) and (−0.3 cm, 0.1 cm).

To find a highly efficient PFSLL with satisfactory focusing performances, two parameters, focusing efficiency and concentration ratio of collection of solar energy, are analyzed with respect to the width d of PFSLL. Here, the focusing efficiency is defined by the ratio of the light collected in a circle with a diameter equivalent to six times full width at half maximum (FWHM) of focus spot to the light intensity at the focusing line after the incident light passes through the lens.[36,37]

And when the incident plane wave with 60° to the central axis focuses on a point at the focal surface AB, the ratio of the incident arc length to the distance from the focal point to the central axis is defined as concentration ratio of collection of energy. With the plate width d of the PFSLL artificially varied from 0.3 cm to 0.5 cm with a step of 0.01 cm, the focusing efficiency and concentration ratio of collection of energy of the PSFLL are investigated at the frequency of 150 GHz, as shown in Fig. 3(a). It shows that as the plate width d of the PFSLL decreases, the focusing efficiency decreases, but the concentration ratio of collection of energy increases instead. The reason for this phenomenon is because the refractive index of the designed PFSLL is affected by the width of the flat plate. It is noted that a compact wave propagation path in the PFSLL can be achieved by shrinking the plate width d, leading to the increasement of concentration ratio of collection of energy. At the same time, the impedance mismatch between the lens and air interface exacerbates, which results in larger scattering and lower focusing efficiency. Based on the above simulated, the change trend of the two parameters is basically completely opposite, considering from the perspective of energy comprehensive, and to better evaluate the focusing effect of PFSLL, here, the produce values of the two parameters is proposed as the energy utilization ratio, as shown in Fig. 3(b). It is clearly seen that the energy utilization ratio first rises and then falls with the plate width d increases from 0.3 cm to 0.5 cm. When the plate width is around 0.4 cm, the energy utilization ratio reaches a peck. Hence, the PFSLL with plate width d of 0.4 cm may be used to design the highly efficient energy concentrator.

The above studies on the PFSLLs' planar focusing performance pave the way for planar focusing array. Then, three PFSLLs are cascaded in a row to make up a planar focusing array to explore its wide-angle focusing characteristics. Figures 4(a)–4(d) show the z component of the electric fields when plane waves with incident angles of 85°, 65°, 55°, and 0° to u axis are incident to the focusing array at 150 GHz, and the red curve is the electric field intensity observed at the focal plane of the array. The blue dotted line shows the focal plane of the array. Obviously, the focusing effect of the array is poor at the plane wave with incident angle of 85° to u axis, of which only the first lens can focus incident wave and collect energy. When the incident angle reduces to 65°, a slightly better focusing effect of the array can be achieved. The results reveal that the designed planar focusing array can achieve beam scanning angle of about ±65°. By comparing the electric field intensity curves of the focusing array's plane with the incident angle of 55° and 0°, it can be found that in order to realize excellent focusing effect, the beam scanning angle should be controlled within ±55°. The PFSLL focusing array based on classical LL can concentrate the light on flat surface of the lens. However, it is not easy to collect light due to the focusing spot close to the lens. The generalized LL, of which focal point can be tuned at outside from the surface of the lens[38] may can solve this disadvantage. Combined with the SC method, a new focusing array with a certain working distance is designed. The z component of the electric fields of the new focusing array at the same incidence angle and frequency are shown in Figs. 4(e)–4(h). It is noted that comparing with the planar focusing array designed by transforming the classical LL and the focal plane of the new focusing array is outside the array. Thus, it provides more accessibility of collecting light. Therefore, the plane focusing array designed by the PFSLL with a plate width of 0.4 cm can achieve a wide-angle focusing and energy collector, which is potential to application in broadband highly efficient energy concentrators.

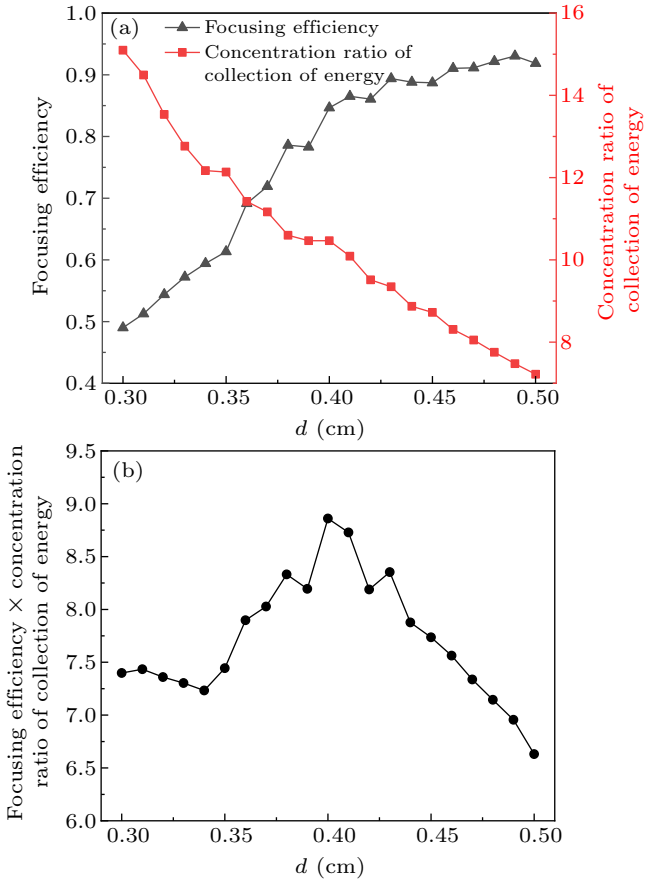


Fig. 3. (a) Focusing efficiency and concentration ratio of collection of energy with different plate width d of PFSLL. (b) Energy collecting ratio (the product of the focusing efficiency and the concentration ratio of collection of energy) with different the plate width d.

Although the LL has been widely used in the field of antennas,[25,39,40] but with the large scanning angle and the ability to accommodate multiple feed sources is still a great challenge. Due to the designed PFSLL with high concentration ratio of collection of energy, the antenna system based on PFSLL can realize the miniaturization of the feeds, which is more conducive to the integration into the on-chip system. In addition, the lens can achieve a large angle scanning beam. To verify the effect, five feed sources as excitation are separately placed on the plane AB from −0.2 cm to 0.2 cm at the same intervals 0.1 cm. Figure 5(a) shows the normalized far-field amplitude of the feed sources at different locations separately

at the frequency 50 GHz. The results verify that when the feed sources are fired simultaneously at different locations, the highly directional plane wave generates in different directions. It is worth noting that the beam scanning range is ±64°. The similar normalized far-field amplitude also respectively calculated at frequencies of 100 GHz, 150 GHz, and 200 GHz, as shown in Figs. 5(b)–5(d). It can be found that as the frequency increases, the range of the beam scanning will decrease slightly but the scanning angle is still more than ±60°. It indicates that the designed PFSLL is capable of achieving wide scanning angle and multibeam. The PFSLL is easy integration and high directionality, so it has great advantages to be applied in the antenna systems as well.

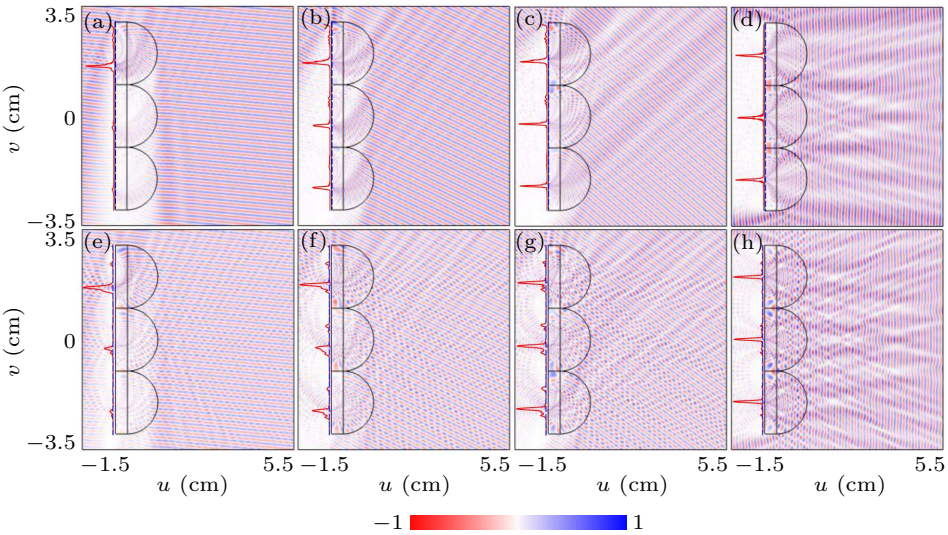


Fig. 4. (a)–(h) The z component of the electric field (perpendicular to the surface of the paper) for plane waves with incident angles of 85°, 65°, 55°, and 0° to u axis at 150 GHz. The red curves are the electric field magnitude of the focusing point observed by the focal plane of the array. The blue dotted line shows the position of the electric field amplitude curve.

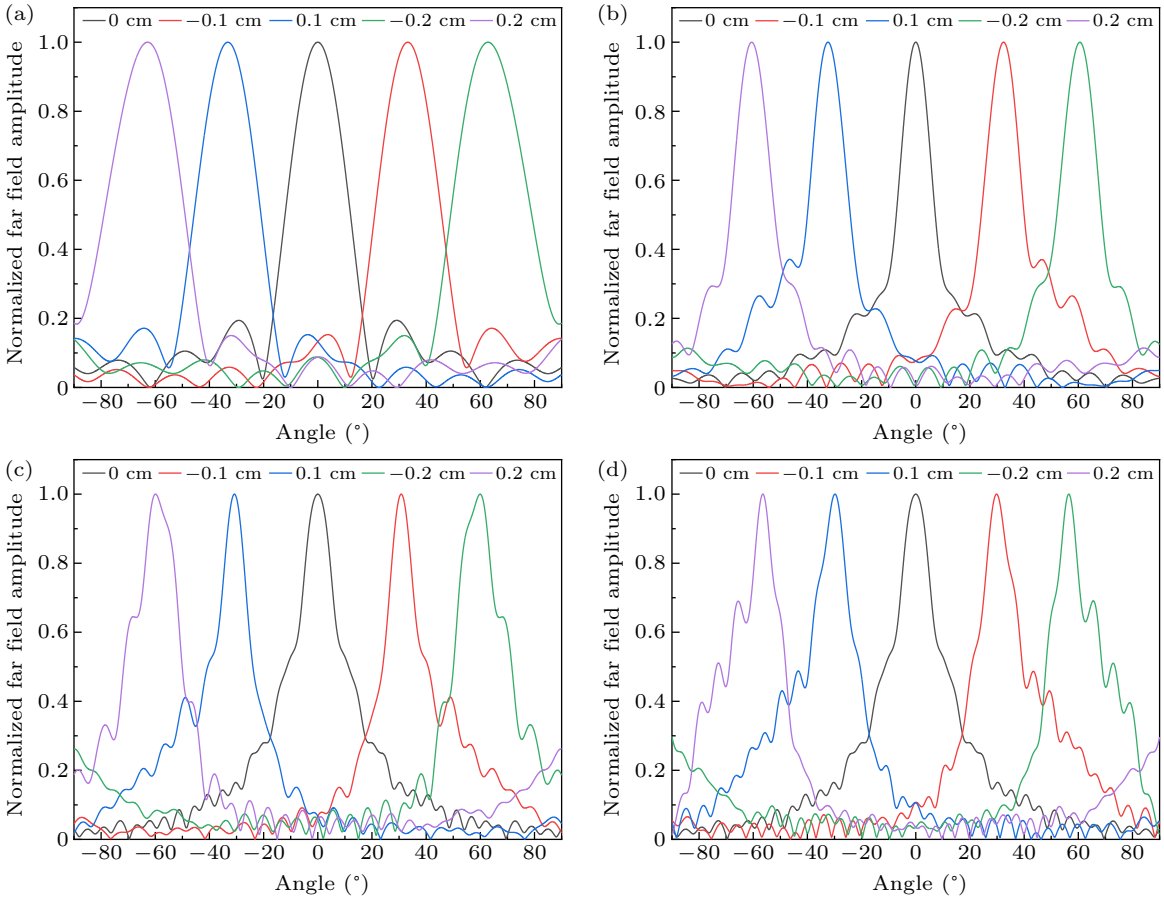


Fig. 5. (a)–(d) The normalized far-field amplitude of five feed sources simultaneously placed for excitation at plane AB with the frequencies of 50 GHz, 100 GHz, 150 GHz, and 200 GHz, and feed sources are placed at an interval of 0.1 cm from −0.2 cm to 0.2 cm (purple is 0.2 cm, blue is 0.1 cm, black is 0 cm, red is −0.1 cm, green is −0.2 cm), respectively.

3. Conclusion

In conclusion, this paper describes the design of PFSLL concentrators with different plane widths using the SC mapping method. Then, the focusing efficiency and concentration ratio of collection of solar energy are calculated by simulation and the results show that the PFSLL has the best focusing effect when the plate width is 0.4 cm. The optimized PSFLL can not only form a plane focusing array with a wide scanning angle, but also realize a multi-beam, wide-bandwidth and wide-angle directional far-field radiation antenna. The focusing properties of the proposed design make it suitable for use in solar concentrator systems and antenna systems.

Acknowledgments

Project supported by the National Key Research and Development Program of China (Grant No. 2020YFA0710100), the National Natural Science Foundation of China (Grant Nos. 92050102 and 11874311), the Shenzhen Science and Technology Program (Grant No. JCYJ20210324121610028), and the Fundamental Research Funds for the Central Universities (Grant Nos. 20720220033 and 20720200074).

References

[1] Parida B, Iniyan S and Goic R 2011 *Renew. Sust. Energ. Rev.* **15** 1625
[2] Sampaio P G V and González M O A 2017 *Renew. Sust. Energ. Rev.* **74** 590
[3] Zhang H, Baeyens J, Degrève J and Cacères G 2013 *Renew. Sust. Energ. Rev.* **22** 466
[4] Li Y, Liao S, Rao Z and Liu G 2014 *Renewable Energy* **69** 34
[5] Chaanaoui M, Vaudreuil S and Bounahmidi T 2016 *Procedia Computer Science* **83** 782
[6] Xu X, Vignarooban K, Xu B, Hsu K and Kannan A M 2016 *Renew. Sust. Energ. Rev.* **53** 1106
[7] Li G, Pei G, Ji J and Su Y 2015 *Appl. Energy* **144** 214
[8] Li G, Pei G, Ji J, Yang M, Su Y and Xu N 2015 *Solar Energy* **120** 565
[9] Li G, Pei G, Yang M, Ji J and Su Y 2014 *Energy Conversion Management* **85** 204
[10] Karp J H, Tremblay E J and Ford J E 2010 *Opt. Express* **18** 1122
[11] Abbas R, Montes M, Piera M and Martínez-Val J 2012 *Energy Conversion Management* **54** 133
[12] Lin M, Sumathy K, Dai Y, Wang R and Chen Y 2013 *Applied Thermal Engineering* **51** 963
[13] Zhu Y, Shi J, Li Y, Wang L, Huang Q and Xu G 2016 *Energy Conversion Management* **126** 89
[14] Abed N and Afgan I 2019 *Adv. Civ. Eng. Tech.* **33** 313
[15] Chafie M, Aissa M F B, Bouadila S, Balghouthi M, Farhat A and Guizani A 2016 *Appl. Thermal Engineering* **101** 273
[16] Mwesigye A, Huan Z and Meyer J P 2016 *Energy Conversion Management* **120** 449
[17] Yin X, Zhu H, Guo H, Deng M, Xu T, Gong Z, Li X, Hang Z H, Wu C and Li H 2019 *Laser Photon. Rev.* **13** 1800081
[18] Yu B, Wen J, Chen X and Zhang D 2019 *Appl. Phys. Express* **12** 092003
[19] Liu Y Q, Ren Z, Shu Y, Wu L, Sun L, Cai H, Zhang X, Lu L, Qi K, Li L, Che Y and Yin H 2022 *Appl. Phys. Express* **15** 014003
[20] Cen Y, Xie J L and Liu J J 2019 *Chin. Opt. Lett.* **17** 080501
[21] Sheng J, Xie J L and Liu J J 2022 *Chin. Opt. Lett.* **18** 120501
[22] Zhao Y Y, Zhang Y L, Zheng M L, Dong X Z, Duan X M and Zhao Z S 2016 *Laser Photon. Rev.* **10** 665
[23] Luneburg R K 1964 *Mathematical Theory of Optics* (University of California Press)
[24] Quevedo-Teruel O and Hao Y 2013 *Opt. Lett.* **38** 392
[25] Mateo-Segura C, Dyke A, Dyke H, Haq S and Hao Y 2014 *IEEE Trans. Anten. Propag.* **62** 1945
[26] Oxburgh S, Tyc T and Courtial J 2014 *Comput. Phys. Commun.* **185** 1027
[27] Demetriadou A and Hao Y 2011 *Opt. Express* **19** 19925
[28] Bor J, Lafond O, Himdi M, Merlet H and Lebars P 2015 *Smooth Plate Luneburg Lens with Superstrate* (IEEE) pp. 1–4
[29] Tang L, Yin J, Yuan G, Du J, Gao H, Dong X, Lu Y and Du C 2011 *Opt. Express* **19** 15119
[30] Schmiele M, Varma V S, Rockstuhl C and Lederer F 2011 *Phys. Rev. A* **81** 033837
[31] Li J, Zhou Y and Chen H 2022 *Chin. Opt. Lett.* **20** 031101
[32] Di Falco A, Kehr S C and Leonhardt U 2011 *Opt. Express* **19** 5156
[33] Zhao P, Cai G and Chen H 2022 *Sci. Bull* **67** 246
[34] Driscoll T A 1996 *ACM Transactions on Mathematical Software* **22** 168
[35] Henrici P 1986 *Applied and computational complex analysis,* Volume 3*: Discrete Fourier analysis, Cauchy integrals, construction of conformal maps, univalent functions*, Vol. 41 (John Wiley & Sons)
[36] Arbabi A, Horie Y, Ball A J, Bagheri M and Faraon A 2015 *Nat. Commun.* **6** 7069
[37] Chen J, Chu H, Lai Y, Chen H, Song W, Chen M and Fang D 2021 *Photon. Res.* **9** 2088
[38] Mao X, Yang Y, Dai H, Luo D, Yao B and Yan S 2015 *Opt. Express* **23** 26426
[39] Hunt J, Tyler T, Dhar S, Tsai Y J, Bowen P, Larouche S, Jokerst N M and Smith D R 2012 *Opt. Express* **20** 1706
[40] Li Y and Zhu Q 2016 *Opt. Express* **24** 7201